

Research Paper

Delivery of miR-146a to Ly6C^{high} Monocytes Inhibits Pathogenic Bone Erosion in Inflammatory Arthritis

Meryem Ammari^{1,10*}, Jessy Presumey^{1,11*}, Clara Ponsolles^{1,12}, Gautier Roussignol², Christine Roubert², Virginie Escriou³, Karine Toupet¹, Anne-Laure Mausset-Bonnefont¹, Maïlys Cren¹, Maxime Robin¹, Philippe Georget⁴, Ramzi Nehmar⁴, Leonie Taams⁵, Joachim Grün^{6,13}, Andrea Grützkau⁶, Thomas Häupl⁷, Yves-Marie Pers^{1,8}, Christian Jorgensen^{1,8}, Isabelle Duroux-Richard¹, Gabriel Courties^{9*}, Florence Apparailly^{1,8}✉*

1. IRMB, INSERM, University of Montpellier, Montpellier, France
2. Exploratory Unit, Sanofi R & D, Montpellier, France
3. UTCBS, CNRS, INSERM, Université Paris Descartes, Sorbonne-Paris-Cité, Chimie ParisTech, PSL Research University, Paris, France
4. Centre de Recherche d'Immunologie et d'Hématologie, INSERM, CNRS, University of Strasbourg, Strasbourg, France
5. Centre for Inflammation Biology and Cancer Immunology, Department of Inflammation Biology, School of Immunology & Microbial Sciences, King's College London, London UK
6. Deutsches Rheuma-Forschungszentrum (DRFZ), Institute of the Leibniz-Association, Berlin, Germany
7. Rheumatologie, La Charité, Berlin, Germany
8. Clinical department for osteoarticular diseases, University hospital of Montpellier, Montpellier, France
9. Center for Systems Biology, Massachusetts General Hospital and Harvard Medical School, 185 Cambridge St, Boston, MA 02114, USA
10. Current address: Avenue Nina Simone, Montpellier, France, ammarimeryem@gmail.com
11. Current address: Children's Hospital, CLS Bldg 3/Carroll Lab, 300 Longwood Ave, Boston MA 02115, USA, email: jessy.presumey@childrens.harvard.edu
12. Current address: Clara PONSOLLES, INSERM unite U1110, 3 Rue Koeberlé, 67000 Strasbourg, France, email: clara.ponsolles@inserm.fr
13. Current address: Dr.JoachimRGruen@T-online.de

* equally contributed

✉ Corresponding author: Florence Apparailly, INSERM unité U1183, Bâtiment IRMB, CHRU Saint Eloi, 80 Avenue Augustin Fliche, 34295 Montpellier, France. Phone: 33-467-335-696, Fax: 33-467-330-113, email: florence.apparailly@inserm.fr.

© Ivyspring International Publisher. This is an open access article distributed under the terms of the Creative Commons Attribution (CC BY-NC) license (<https://creativecommons.org/licenses/by-nc/4.0/>). See <http://ivyspring.com/terms> for full terms and conditions.

Received: 2018.08.17; Accepted: 2018.10.12; Published: 2018.11.13

Abstract

Rationale: Monocytes play critical roles in the pathogenesis of arthritis by contributing to the inflammatory response and bone erosion. Among genes involved in regulating monocyte functions, miR-146a negatively regulates the inflammatory response and osteoclast differentiation of monocytes. It is also the only miRNA reported to differentially regulate the cytokine response of the two classical Ly6C^{high} and non-classical Ly6C^{low} monocyte subsets upon bacterial challenge. Although miR-146a is overexpressed in many tissues of arthritic patients, its specific role in monocyte subsets under arthritic conditions remains to be explored.

Methods: We analyzed the monocyte subsets during collagen-induced arthritis (CIA) development by flow cytometry. We quantified the expression of miR-146a in classical and non-classical monocytes sorted from healthy and CIA mice, as well as patients with rheumatoid arthritis (RA). We monitored arthritis features in miR-146a^{-/-} mice and assessed *in vivo* the therapeutic potential of miR-146a mimics delivery to Ly6C^{high} monocytes. We performed transcriptomic and pathway enrichment analyses on both monocyte subsets sorted from wild type and miR-146a^{-/-} mice.

Results: We showed that the expression of miR-146a is reduced in the Ly6C^{high} subset of CIA mice and in the analogous monocyte subset (CD14⁺CD16⁻) in humans with RA as compared with healthy controls. The ablation of miR-146a in mice worsened arthritis severity, increased osteoclast differentiation *in vitro* and bone erosion *in vivo*. *In vivo* delivery of miR-146a to Ly6C^{high} monocytes, and not to Ly6C^{low} monocytes, rescues bone erosion in miR-146a^{-/-} arthritic mice and reduces osteoclast differentiation and pathogenic bone erosion in CIA joints of miR-146a^{+/-} mice, with no effect on inflammation. Silencing of the non-canonical NF-κB family member RelB in miR-146a^{-/-} Ly6C^{high} monocytes uncovers a role for miR-146a as a key regulator of the differentiation of Ly6C^{high}, and not Ly6C^{low}, monocytes into osteoclasts under arthritic conditions.

Conclusion: Our results show that classical monocytes play a critical role in arthritis bone erosion. They demonstrate the theranostics potential of manipulating miR-146a expression in Ly6C^{high} monocytes to prevent joint destruction while sparing inflammation in arthritis.

Key words: monocyte subsets, miR-146, osteoclast, bone erosion, arthritis

Introduction

Rheumatoid arthritis (RA) is an autoimmune disease of unclear etiology. It is characterized by a chronic systemic inflammation, mainly affecting joints and leading to progressive and destructive polyarthritis [1, 2]. Since interactions between inflammation and bone metabolism might be manipulated as therapies for RA, the identification of key cellular and molecular mechanisms underlying these interactions is necessary.

Monocytes are plastic cells that can differentiate into dendritic cells (DCs), macrophages (M ϕ) and osteoclasts (OCs), thus controlling both inflammation and bone turnover. Excessive activation and abundance of monocytes are crucial to RA disease progression, contributing to both chronic inflammation and bone destruction [3]. Monocytes accumulate in the blood and continuously migrate into the inflamed joints [4] where they acquire an activated phenotype and promote Th17 differentiation [5, 6], perform local antigen-presentation and osteoclastogenesis [7]. Monocyte number correlates with disease severity [8, 9] and with the efficacy of therapies [10-12]. However, the mechanisms involved in the link between inflammation and bone erosion are still poorly understood.

Monocytes comprise two main subsets committed to different functions [13-15], namely the "classical" mouse inflammatory Ly6C^{high} and the "non-classical" patrolling Ly6C^{low} monocyte subsets, and their human CD14⁺CD16⁻ and CD14^{dim}CD16⁺ counterparts, respectively [13, 16]. Ly6C^{high} monocytes secrete inflammatory mediators, are specialized in bacterial defense and can differentiate into macrophages, inflammatory DCs and OCs [17-19]. Ly6C^{low} monocytes survey endothelial cells and surrounding tissues for damage or viral infection and are involved in tissue repair [13]. Previous reports involved either Ly6C^{low} or Ly6C^{high} monocytes in the initiation of joint inflammation, depending on the experimental model used [20-22]. Although these studies have underscored the importance of studying monocyte subsets in arthritis, and relevance of using monocytes for theranostics in arthritis has been documented [23], factors that control the pathogenic role of monocyte subsets remain poorly explored.

Among molecular rheostat involved in cellular activation and differentiation, micro(mi)RNAs play important roles. They are small, noncoding RNA molecules that regulate genetic programs at the post-transcriptional level [24, 25]. Abnormal expression of miRNAs has been implicated in RA, where they might represent promising biomarkers and innovative target genes [26]. The role of miRNAs in regulating monocyte differentiation into M ϕ and

DCs has been documented, but little is known about how they influence their differentiation into OCs. A few groups have addressed this issue in bone physiology and disease [27-30], however not in the context of functional heterogeneity of monocyte subsets. So far, miR-146a is the only miRNA identified as regulating functional heterogeneity of monocyte subsets, controlling the amplitude of the inflammatory response of Ly6C^{high} (but not Ly6C^{low}) monocytes during bacterial infection [31]. MiR-146a is a well-known negative regulator of inflammation in monocytes/macrophages [32] and of osteoclastogenesis [33] but is elevated in RA blood and synovial tissue [34-36]. It has been shown that miR-146a deletion aggravates joint inflammation in the experimental mouse models of Lyme-induced arthritis and human TNF-transgenic arthritis [37, 38]. Finally, administration of miR-146a mimics reduces joint destruction in mice with collagen-induced arthritis (CIA) [33]. Although these studies highlighted the therapeutic potential of manipulating miR-146a to control bone destruction and inflammation in arthritis, the role of miR-146a in monocyte subsets has not been addressed in the context of arthritis. Therefore, the present study aimed at investigating whether and how miR-146a expression in inflammatory Ly6C^{high} monocytes influence the inflammation and bone erosion during arthritis development, and at evaluating its theranostics potential.

Materials and methods

Ethics statement

DBA/1 mice were obtained from Harlan laboratories, wild-type (WT) C57BL/6 and miR146a-KO (B6(FVB)-Mir146^{tm1.1Bal/J}) mice were purchased from Charles River (France). Experimental groups were obtained by crossing heterozygous mice to obtain WT and miR146a-KO littermates with the same genetic background. Animals were maintained in specific pathogen free conditions. Experiments were performed in accordance with EU directive 2010/63/EU and approved by the Ethics Committee for Animal Research of Languedoc-Roussillon (00920.01) and French health authorities (C34-172-36). For RA patients and healthy controls, informed consents were provided in accordance with procedures approved by the local human ethics committee (ID RCB 2008-A01087-48) and with the code of ethics of the world medical association. Fresh peripheral blood (PB) was obtained from healthy donors with no history of autoimmune diseases and from RA patients with a 28-joint-count Disease Activity Score (DAS28) \geq 5.1. PB and synovial fluid (SF) samples were obtained from patients with RA following informed consent at

Guy's Hospital, London UK (Bromley Research Ethics Committee: 06/Q0705/20).

Flow cytometry and cell sorting

The monoclonal antibodies used for mouse and human experiments were purchased from BD Biosciences, eBioscience and BioLegend (see supplemental information). Human monocytes were identified as CD19⁻, CD3⁻, CD56⁻, SSC^{low}, and CD14^{high}/CD16^{low} (classical monocytes), or CD14^{low}/CD16^{high} (non-classical monocytes). Mouse monocytes subsets were identified as Ly6G⁻, CD11b⁺ CD115⁺, Ly6C^{high/low} (Figure S1). Macrophages from the joints were defined as Ly6G⁻, CD11b⁺, F4/80^{high}, Ly6C^{low}. Neutrophils were defined as CD11b⁺ Ly6G⁺. For dead cell exclusion, DAPI was used (Sigma-Aldrich).

For mouse studies, blood and spleen samples were treated for 4 min with RBC and ACT red blood cell lysis buffer, respectively. For intracellular TNF staining, cells (1×10^6 cells/well in 96-well plate) were stimulated for 3h with PMA (50ng/ml, Sigma) and ionomycin (250ng/ml, Sigma). Brefeldin A (10 μ g/ml, Sigma) was added during the stimulation. Cells were stained for appropriate cell surface markers prior to fixation and permeabilization using the Cytotfix/Cytoperm kit (BD Pharmingen) according to manufacturer's protocols. Intracellular staining was performed using APC-conjugated anti-TNF- α (clone MP6-XT22; BD Biosciences). For human blood samples, PBMCs were prepared on a Ficoll-Hypaque density gradient (Amersham). For cell isolation from mouse joint tissue, hind paws were harvested. The skin and soft tissues were carefully removed and the ankle joints were cut off before the tibial muscle. Joints were then digested with 1 mg/mL of Collagenase D (Roche) for 1 hour at 37°C. Cells were then filtered using a 40 μ m nylon cell strainer (BD Falcon) and used for FACS analyses. Then, the antibody staining was performed according to the manufacturer's instructions. When indicated, monocytes were FACS-sorted on a BD FACSAria Cell Sorting System (BD Biosciences) with >97% purity by the Montpellier RIO imaging IGMM - Cytometry platform. Splenic CD11b cells were isolated using the CD11b Microbeads (Miltenyi Biotec). For some experiments, blood CD14⁺ monocytes were negatively selected (purity > 97%) from PBMCs by magnetic separation (Dynabeads Untouched Human Monocytes, Invitrogen) isolated from healthy individuals or rheumatoid arthritis (RA) patients, according to the manufacturer's instructions.

Induction of arthritis models and clinical evaluation

The collagen-induced arthritis (CIA) mouse

model was performed using 9 week-old DBA/1 male mice. CIA was induced as previously described [40] using bovine type II collagen from MD Biosciences (Zurich, Switzerland), acetic acid from Sigma-Aldrich, and Freund's adjuvants from Pierce (Bezons, France). Mice were injected intravenously from the indicated starting day, either once or weekly during 3 weeks, with 0.5 mg/kg of miR-146a mimics (miRIDIAN mmu-miR-146a, Fermentas GmbH, Germany) formulated as lipoplexes with the DMAPAP/DOPE cationic liposome as previously described [39]. Controls were injected with lipoplexes containing irrelevant miRNA mimics. The serum transfer arthritis model (STA) was performed using 7-week-old C57BL/6 male mice injected intraperitoneally (i.p.) twice with 150 μ l of arthritogenic serum obtained from K/BxN mice (day 0 and 1). Non-arthritic control mice were injected i.p. with PBS. For both models, paw thickness was blindly measured with a Mitutoyo micrometer (Sigma-Aldrich) thrice a week. At euthanasia, paws and knees were fixed in PBS-PFA 4%, decalcified with PBS-EDTA 14%, and embedded in paraffin. Ten successive sections of 5 μ m were stained with Safranin O/Fast green. Erosion was qualitatively evaluated blindly and scored as previously described [40]. 5 μ m paraffin knee sections were de-paraffined (xylene), rehydrated and stained with TRAP staining buffer for 20 minutes at 37 °C, and co-stained with hematoxylin. Stained sections were scanned using an NDP Nanozoomer HT (Hamamatsu). TRAP positive osteoclast precursors and mature osteoclasts were visually counted in the pannus.

Osteoclast differentiation

For bone marrow-derived progenitor cells, bone marrow was flushed and cultured in α -MEM containing 10% heat-inactivated FCS for 24 hours. Non-adherent cells were collected and cultured in complete medium, supplemented with 15 ng/ml M-CSF to induce BMDM (Bone Marrow Derived Macrophages) differentiation at (5×10^5 cells/500 μ l in 48 wells plate). After 48 hours, medium was changed and replaced by complete medium supplemented with 40 ng/ml RANKL and 15 ng/ml M-CSF and replaced every two days for extended time (Miltenyi Biotec).

For TRAP staining, cells were fixed with PBS-PFA 4%, permeabilized with 1:1 ethanol and acetone mixture, and stained for Tartrate-resistant acid phosphatase (TRAP) [41]. Nuclei were stained with DAPI dye. Cells were observed and counted automatically using a Cellomics Arrayscan VTI (Thermo Scientific, Saint Herblain, France). TRAP⁺ cells with more than three nuclei were considered as

mature osteoclasts. For functional analysis of bone resorption, cells were cultured on Osteo Assay Surface plates for 7 days (Corning) and then removed by bleaching. The surface of mineralized matrix degraded was quantified using image J software and relative resorption area was expressed as a percentage of total surfaces analyzed.

Quantitative Real-time PCR

For human and mouse gene analyses, total RNA including small RNAs was extracted using miRNeasy mini kit and the QIAcube automate according to the manufacturer's instructions (QIAGEN). The expression levels of miRNA and mRNA were quantified using the Taqman microRNA and gene expression assays (Life Technologies), respectively. Taqman gene expression assays were used for mouse *Relb* (Mm00485664_m1), *Traf6* (Mm00493836_m1), and *Acp5* (Mm00475698_m1) mRNAs. We used house-keeping genes for normalization including RNU48 for human miR-146a, snoRNU6B and snoRNU135 for mouse miR-146a, and *gapdh* for osteoclast genes. Real time PCR were performed Analyses were performed using Rotor-gene Q software (QIAGEN). Relative gene expression was calculated using the comparative threshold cycle (C_T) method.

Microarray hybridization and data analysis

Total RNA of Ly6C^{low} and Ly6C^{high} monocytes isolated from blood samples of miR-146a^{-/-} mice or control littermates were extracted using RNeasy mini kit (Qiagen). The generation of cRNA, sample hybridization (using Affymetrix GeneChip Mouse 430_2 arrays) and scanning with a GeneChip Scanner 3000 (Affymetrix) were performed as described previously [42] and data were analyzed using BioRetis database (c.f. supplemental information). For identification of new potential miR-146a-target mRNAs associated with osteoclast differentiation and function, we used PathCards software for selection of genes specific for osteoclast differentiation pathway [43]. We used the VENNY interactive tool (<http://bioinfogp.cnb.csic.es/tools/venny/index.html>) to obtain common genes between osteoclast differentiation pathways, genes modulated in KO versus WT Ly6C^{high} monocytes, and genes differentially expressed between both monocytes subsets under steady state conditions.

In vivo bone histomorphometric analysis

Micro-computed tomography was performed using the Skyscan 1176 microCT system on living mice (Bruker microCT, Belgium). At indicated time, mice legs were scanned using the following settings: isotropic voxels size of 18 μ m, voltage of 50 kV, current of 500 mA, 0.5 mm aluminium filter, 180

degrees with a 0.7 degree rotation step and a 210 ms exposure time. Data were reconstructed using NRecon software (Bruker microCT, Belgium). Quantification of 3 bone parameters (BV/TV, BS/BV and Tb.Th) was performed on the trabecular region of the proximal part of each femur (CT Analyzer software, Bruker microCT, Belgium).

Statistical analyses

GraphPad prism software was used to perform statistical analysis. Unpaired Mann-Whitney or paired Wilcoxon non-parametric tests were used to compare two groups. One-way ANOVA followed by Fisher's post-test analysis or Kruskal-Wallis test were used for statistical comparisons of more than two groups. Two-way repeated measures ANOVA followed by Tukey's post-test analysis were performed for kinetic comparisons. P values less than 0.05 were considered statistically significant.

Results

Collagen-induced arthritis is associated with Ly6C^{high} monocytosis

We first performed an in-depth study of the temporal changes in monocyte subsets during progression of the mouse CIA. In full-blown arthritic mice (40 days after induction), the number of blood Ly6C^{high} monocytes was increased as compared with control mice (Figure 1A). A kinetic study of the frequency of circulating subsets showed a 2-fold increase in Ly6C^{high} monocytes before the clinical onset, whereas the frequency of Ly6C^{low} monocytes remained unchanged, as compared with non-immunized (NI) mice (Figure 1B). The total number of leukocytes did not change (data not shown). In the spleen, the frequency of Ly6C^{high} monocytes was also transiently increased after the boost (day 21 post-immunization) while the frequency of Ly6C^{low} monocytes did not significantly change during CIA development (Figure 1C). Although already present in joints under healthy conditions (NI), leukocytes markedly infiltrated joints of CIA mice (Figure 1D). There were 15 times more Ly6C^{high} monocytes into the arthritic joints than in healthy joints, associated with increased number of M ϕ . Ly6C^{low} monocytes were under-represented compared to Ly6C^{high} monocytes ($7.1 \pm 0.7 \times 10^3$ versus $48 \pm 9 \times 10^3$ cells/joint, respectively). As previously reported [20], a substantial neutrophil infiltration was also observed into the arthritic joints. We showed that Ly6C^{high} monocytes infiltrating the joint tissue of arthritic mice produced TNF- α and displayed an activated phenotype while those from NI mice did not (Figure 1E). Altogether, our data are indicative of a selective

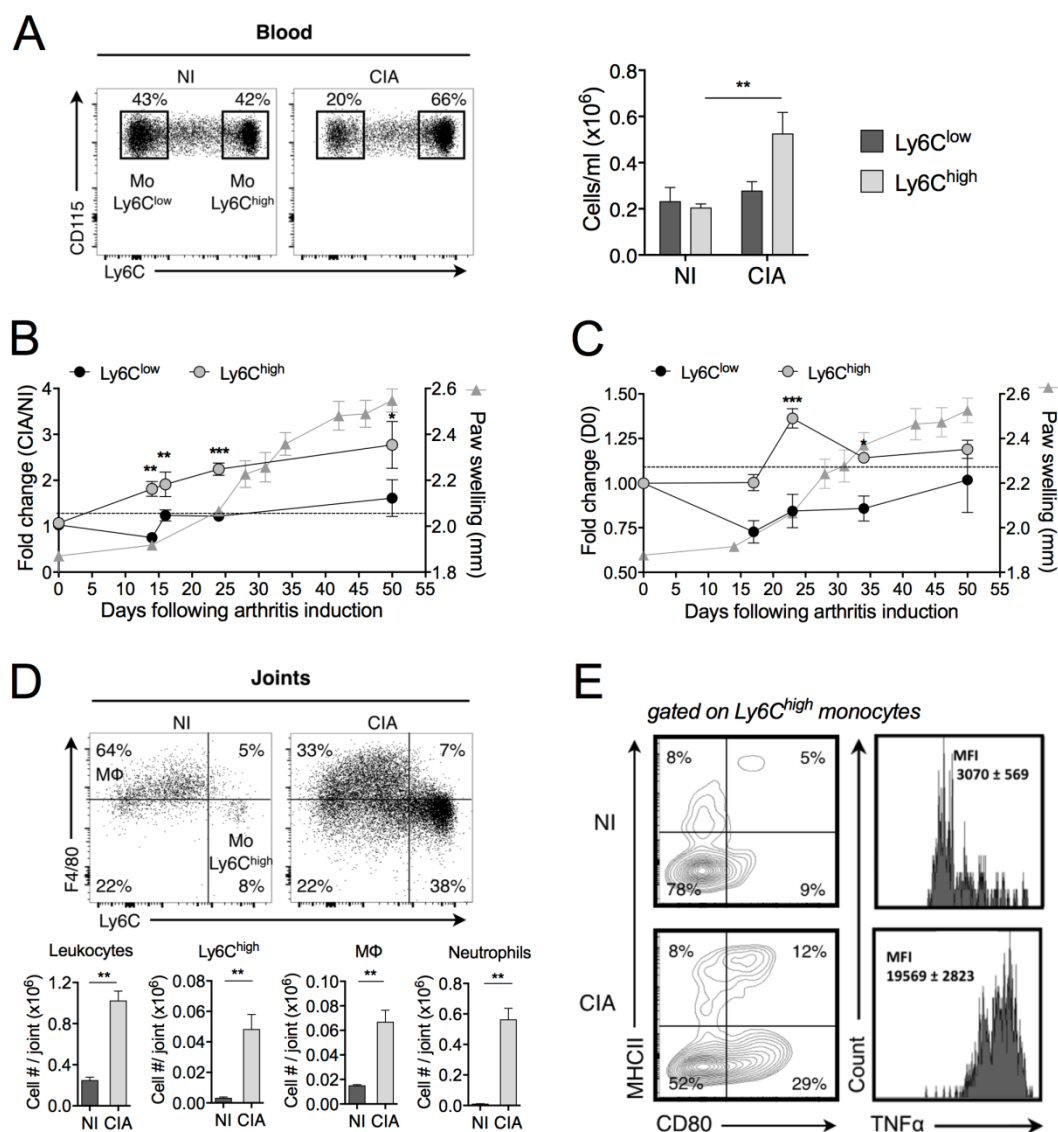


Figure 1. Inflammatory Ly6C^{high} monocytes are amplified in arthritis. DBA/1 mice were immunized with bovine type II collagen and boosted on day 21 to induce collagen-induced arthritis (CIA). Non-immunized (NI) DBA/1 mice were used as controls. (A) Mice were sacrificed 40 days after immunization and frequencies of Ly6C^{high} (grey symbols) and Ly6C^{low} (black symbols) monocytes quantified in the blood. (B-C) Temporal changes in Ly6C^{high} and Ly6C^{low} monocyte subsets were quantified in peripheral blood (B) and spleen (C), compared to day 0 of arthritis. Arthritis severity was assessed by measuring the hind-paw swelling for each mouse along the course of the disease (grey triangles). (D) At day 50 post-immunization, leukocytes were isolated from ankle joints of CIA (grey bars) and NI (dark bars) mice. Representative dot plots for F4/80^{high} macrophages and Ly6C^{high} monocytes are shown (gated on CD45⁺ Ly6G⁻ CD11b⁺ cells). Bar graphs show flow cytometric enumeration of Ly6C^{high} monocytes (Mo Ly6C^{high}), macrophages (MΦ) and neutrophils. (E) Activation status of Ly6C^{high} monocytes from ankle joints was assessed by membrane staining of CD80 and MHCII and TNF-α intracellular cytokine staining. The gates were set using isotype control antibodies. The frequency at each time point represents the mean ± SEM of 3-8 mice/group. Differences between groups were compared using two-way ANOVA (A), two-way repeated measures ANOVA (B, C), and non-parametric Mann-Whitney test (D). ** p<0.01, *** p<0.001.

expansion of Ly6C^{high} monocytes in the peripheral blood and spleen of CIA mice, starting before disease onset and gradually progressing with enhanced disease severity, which are mobilized to the inflamed joints and express an inflammatory profile, whereas such changes were not observed for Ly6C^{low} monocytes. This suggests a critical role of Ly6C^{high} monocytes in pathogenesis of CIA.

Expression of miR-146a is decreased in inflammatory monocytes of arthritic individuals

Since miR-146a plays important regulatory roles

in the development and functions of monocytes, we assessed the expression levels of miR-146a in the context of monocytes' heterogeneity and disease. In monocyte subsets sorted from the blood of healthy mice, miR-146a was 120-fold more expressed in Ly6C^{low} monocytes than in Ly6C^{high} monocytes (Figure 2A). Interestingly, miR-146a expression also displayed the highest difference between both monocyte subsets isolated from the spleen (data not shown). Consistent with findings that human CD16⁺ monocytes resemble mouse Ly6C^{low} monocytes, miR-146a was also detected at higher levels in blood

CD16⁺ monocytes (18-fold) than in CD14⁺ monocytes, which resemble mouse Ly6C^{high} monocytes (Figure 2B). The expression level of miR-146a tended to decrease in Ly6C^{high} monocytes of CIA mice compared with healthy mice (Figure 2C). Importantly, a significant reduction was also found in CD14⁺ monocytes isolated from the blood of patients with RA, compared with healthy controls, and in 3 out of 4 patients the expression levels in synovial fluid CD14⁺ monocytes were reduced compared to peripheral blood counterparts (Figure 2D-E). The expression of miR-146a in Ly6C^{low} monocytes was also reduced under arthritic conditions (10-fold, data not shown). Interestingly, miR-146a was expressed in other types of blood cells such as NK, granulocytes, T and B cells, but no difference was observed between RA and controls (Figure S2). These results suggest that a reduction of miR-146a expression in inflammatory monocytes might be involved in the increase of inflammation and osteoclast-dependent bone resorption under arthritic conditions.

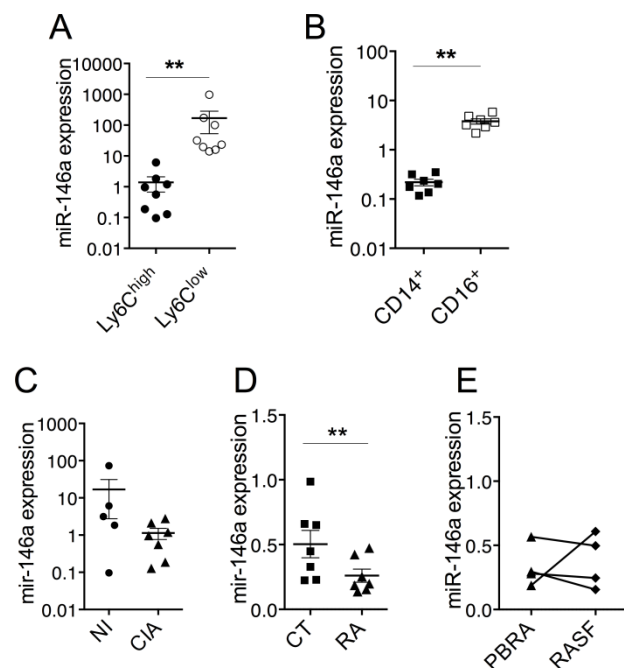


Figure 2. Expression of miR-146a by Ly6C^{high} monocytes is decreased in arthritic individuals. Monocyte subsets were FACS sorted from mouse and human samples, isolated from either healthy or arthritic individuals. Relative miR-146a expression was quantified using RT-qPCR in (A) Ly6C^{high} (black circles) or Ly6C^{low} (white circles) monocytes isolated from blood of healthy mice, (B) CD14⁺ (black squares) and CD16⁺ (white squares) monocytes isolated from blood samples collected from healthy donors, (C) Ly6C^{high} monocytes isolated from healthy (NI, black circles) mice and collagen-induced arthritic (CIA, black triangles) mice, (D) CD14⁺ monocytes isolated from the blood of either healthy donors (CT, black squares) or patients with rheumatoid arthritis (RA, black triangles). (E) Relative miR-146a expression was quantified using RT-qPCR in CD14⁺ monocytes isolated from the peripheral blood (PBRA, black diamonds) or synovial fluid (RASf, black triangles) of RA patients. Data are presented as mean \pm SEM of 3-8 biological replicates corresponding to either individual (human) or 20-25 pooled (mice) samples. Two-tailed Wilcoxon test (A-B, E) and Mann-Whitney test (C-D) were used. ** $p < 0.01$, ns: not significant.

miR-146a deficiency enhances inflammatory arthritis severity and bone erosion

Considering the negative regulatory role of miR-146a in inflammation and osteoclastogenesis, we hypothesized that mice lacking miR-146a would develop more severe arthritis compared to wild type (WT) littermates. Therefore, we used the K/BxN serum transfer arthritis model (STA) [45]. As expected, absence of miR-146a worsened disease severity, as evidenced by increased arthritic score in miR-146a^{-/-} mice compared with WT littermates (Figure 3A). Since miR-146a was reported to control frequency and pro-inflammatory responses of Ly6C^{high} monocytes to bacterial challenge [31], we monitored these parameters under autoimmune conditions. We were not able to detect differences in monocyte subsets frequencies or pro-inflammatory cytokine production (data not shown). Histopathological analyses of serial knee sections however revealed a 2-fold higher number of osteoclasts involved in joint destruction in the pannus of miR-146a^{-/-} mice compared with miR-146a^{+/+} littermates as assessed by the quantification of tartrate resistant acid phosphatase (TRAP)-positive cells located at the cartilage-synovial interface (Figure 3B). Micro-computed tomography analyses of the proximal femur of arthritic mice revealed that global miR-146a deletion significantly reduced bone mass (BV/TV) by 22% and trabecular thickness (Tb.Th) by 10% compared with miR-146a^{+/+} littermates (Figure 3C, grey bars). Interestingly, the trabecular bone parameters remained unchanged in healthy miR-146a^{-/-} mice as compared with WT littermates (Figure 3C, black bars).

Ex vivo osteoclast differentiation assays were performed with both bone marrow and splenic osteoclast progenitors (OCPs) isolated from either miR-146a^{-/-} or miR-146a^{+/+} arthritic mice. Deletion of miR-146a from both bone marrow and splenic CD11b⁺ precursors increased osteoclastogenesis compared with miR-146a^{+/+} OCPs (Figure 3D). The magnitude and speed of the OC differentiation was higher and faster when using splenic CD11b⁺ than BM as progenitors. TRAP⁺ osteoclast number was also augmented in cultures of BM miR-146a^{-/-} progenitors isolated from arthritic mice compared to healthy miR-146a^{-/-} controls (160%, Figure 3E), to a level comparable to the osteoclast number obtained when comparing miR-146a^{-/-} versus miR-146a^{+/+} progenitors from arthritic mice (142%, Figure 3D right panel). Together, our results show that under arthritic conditions, but not under physiological conditions, miR-146a is crucial in regulating osteoclast progenitors and bone resorption.

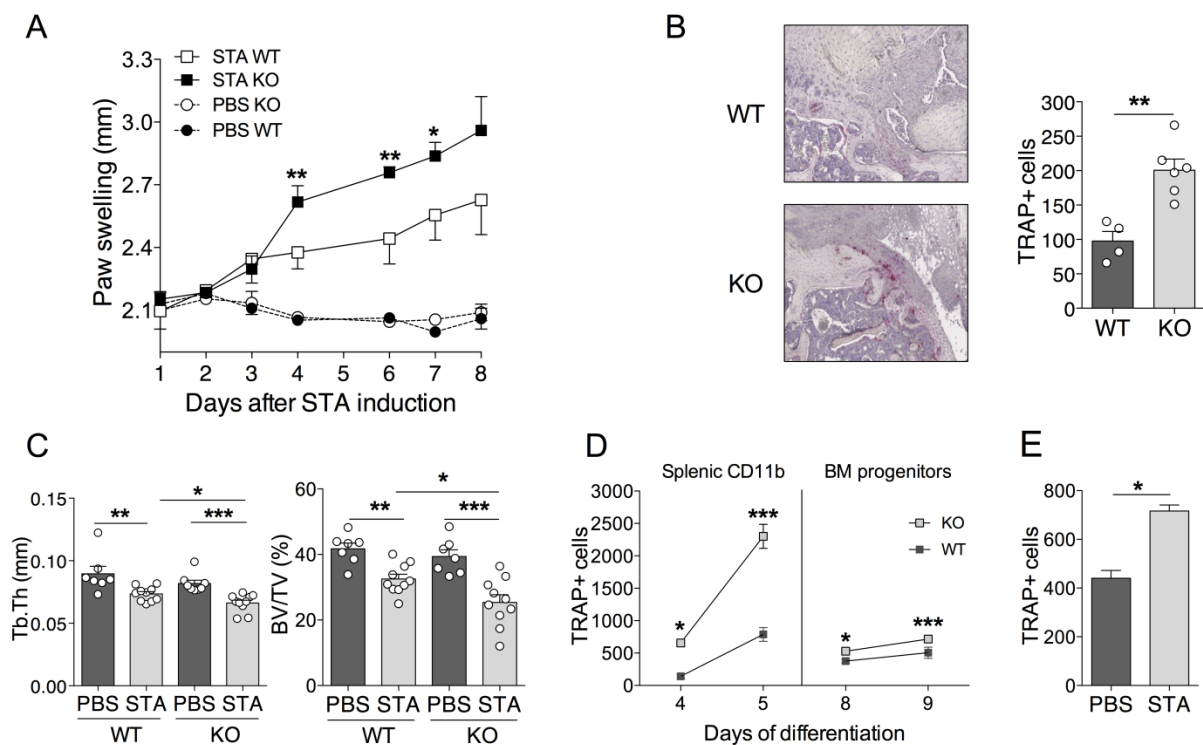


Figure 3. MiR-146a deficiency increases osteoclast differentiation and inflammatory arthritis-induced bone erosion. miR-146a^{-/-} (KO) mice or wild type (WT) littermates were injected i.p. on day 0 and 1 with K/BxN serum to induce serum-transfer arthritis (STA). Control groups were injected with PBS. Mice were sacrificed 11 days after the first injection (n=4-10 mice/group). **(A)** Arthritis severity was monitored. Significant differences to the wild-type group are marked. Data are representative of four independent experiments. **(B)** Knee sections were processed for TRAP and hematoxylin staining. Representative sections are shown (5x magnification). The number of TRAP positive osteoclast cells was counted at pannus site. **(C)** Micro-computed tomography analysis was performed at day 10 for 3-dimensional reconstruction of the anklebones and quantification of trabecular micro-architecture parameters of proximal femur bone, including trabecular thickness (Tb.Th, mm) and bone volume (BV/TV, %). **(D)** Temporal changes in osteoclast differentiation capacity of splenic and bone marrow precursors isolated from arthritic miR-146a KO or WT mice were monitored at the indicated time points. The number of TRAP-positive multinucleated osteoclasts was quantified using automated fluorescence imaging (n=20 areas/well, n=4 mice/group). **(E)** Osteoclast precursors from STA or PBS miR-146a^{-/-} (KO) mice were cultivated in osteoclast differentiation medium for 7 days. Number of TRAP-positive multinucleated osteoclasts was quantified using automated fluorescence imaging (n=20 areas/well, n=4 mice/group). Osteoclast differentiation potential of miR-146a deficient progenitors isolated from arthritic or healthy mice after 9 days of culture (n=4). Data are presented as mean ± SEM and representative of four independent experiments. Differences between groups were compared using two-way repeated measures ANOVA (A), Mann-Whitney test (B and E), or two-way ANOVA (C, D) * p<0.05, ** p<0.01, *** p<0.001.

To determine whether the impact of miR-146a deficiency on bone destruction was dependent on joint inflammation, we used the ovariectomy-induced osteoporosis (OVX) mouse model to challenge bone remodeling without inflammation. Reduction of uterine weight in all ovariectomized mice indicated efficient oestrogen depletion (Figure S3A). As expected, WT CD11b⁺ precursors isolated from OVX mice displayed increased osteoclast differentiation compared to sham-OVX mice (Figure S3B). In addition, miR-146 deficiency increased the numbers of TRAP⁺ osteoclasts in sham-KO controls as compared with sham-WT group. The numbers of TRAP⁺ multinucleated osteoclasts remained unchanged when miR-146 deficient mice were ovariectomized (Figure S3B). *In vivo*, bone morphometric parameters were also unaltered by the absence of miR-146a in OVX-induced osteoporosis as compared with sham-OVX controls (Figure S3C). Our *in vivo* data suggest that the absence of miR-146a does not impair physiological bone architecture nor ovariectomy-induced osteoporosis, but increases

inflammation-induced bone resorption and reduces bone mass, at least in part through increased osteoclastogenesis, in the context of arthritis.

In vivo delivery of miR-146a to Ly6C^{high} monocytes attenuates bone erosion in arthritis

To determine whether these effects were mediated by reduced miR-146a-regulated pathways in Ly6C^{high} monocytes, we took advantage of the DMAPAP/DOPE cationic liposome that we previously developed to deliver RNAi triggers to Ly6C^{high} monocytes, and not to Ly6C^{low} monocytes, upon intravenous injection [39]. We used the collagen-induced arthritis (CIA) mouse model that is the gold-standard model of RA to address questions of disease pathogenesis and validate new therapies. First, efficient delivery of miR-146a mimics to Ly6C^{high} monocytes was validated. The expression level of miR-146a was 7-fold increased in the Ly6C^{high} monocyte subset sorted from arthritic mice 72 hours after a single intravenous injection of miR-146a mimics-containing lipoplexes as compared to Ly6C^{low} monocytes (Figure 4A). Next, we investigated the

effect of ectopic miR-146a expression in Ly6C^{high} monocytes on disease severity and joint histopathology. Weekly administration of miR-146a mimics-containing lipoplexes from day 18 over 3 weeks time increased 60-fold the expression of miR-146a in the Ly6C^{high} monocytes as compared to controls (Figure 4B). Targeting miR-146a in Ly6C^{high} monocytes was neither effective in reducing disease severity, Ly6C^{high} frequencies, nor pro-inflammatory cytokine secretion (Figure S4A-C). However, compared with controls, mice injected with miR-146a mimics showed a reduced number of OCs accumulated within the synovial pannus and decreased local bone erosion (Figure 4C-D).

To test *in vivo* whether the Ly6C^{high} subset is responsible for increased bone loss in miR-146a^{-/-} mice under arthritic conditions, we rescued miR-146a expression in Ly6C^{high} monocytes using the DMAPAP/DOPE cationic liposome. Again, enforced expression of miR-146a in Ly6C^{high} monocytes was

not effective in reducing arthritis severity, Ly6C^{high} frequencies, or pro-inflammatory cytokine secretion in the STA model (Figure S4D-F). Micro-computed tomography analyses however evidenced an efficient rescue of the KO phenotype on bone erosion, as assessed by reduced bone specific surface (BS/BV) and increased trabecular thickness (Tb.Th) in miR-146a-treated mice compared with miRNA control-injected KO mice (Figure 4E). Importantly, bone morphometric characteristics reached levels of those observed in miR-146a^{+/+} littermates injected with miRNA control. Overall, using two arthritic mouse models, our results indicate that specific over-expression of miR-146a in Ly6C^{high} monocytes is sufficient to impede bone erosion during inflammatory arthritis. Our findings also suggest that, in the context of arthritis and miR-146a, Ly6C^{high} monocytes play a role in osteoclastogenesis and not in inflammation, and that this effect might be at least in part cell-intrinsic.

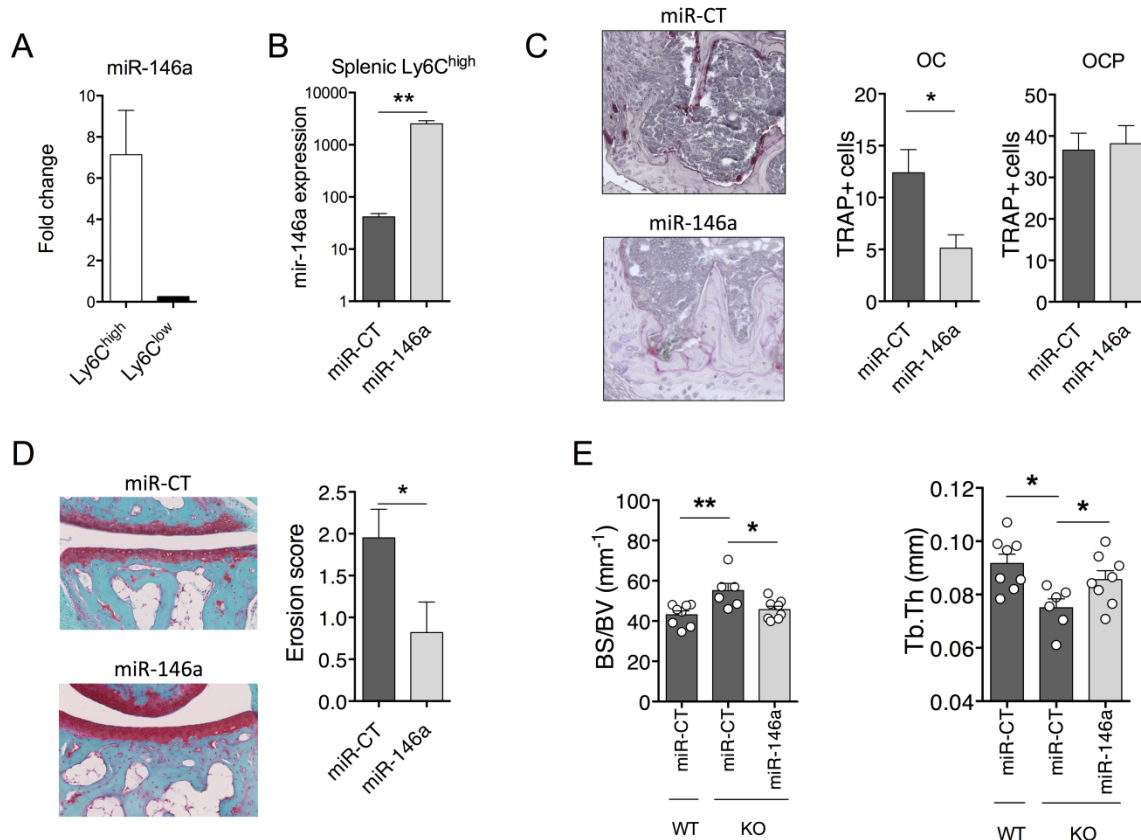


Figure 4. *In vivo* delivery of miR-146a mimics to Ly6C^{high} monocytes interferes with pathogenic bone erosion during inflammatory arthritis in wild type and knockout mice. (A-D) The DMAPAP/DOPE cationic liposome was formulated with either miR-146a mimics (miR-146a) or non-targeting miRNA mimics (miR-CT) and injected (0.5mg/kg) either only once (A), twice (B), or weekly over a 3-weeks period (C-D) from day 23. Mice were sacrificed 24 hours after the last injection. DBA/1 mice were immunized with bovine type II collagen and boosted on day 21. (A) Fold change of miR-146a expression in splenic Ly6C^{high} and Ly6C^{low} monocyte subsets isolated from pooled mice injected with miR-146a mimic-containing lipoplexes compared to miR-CT mimic-injected animals. (B) Expression level of miR-146a in splenic Ly6C^{high} monocytes following treatment with either miR-146a mimics- or miR-CT mimics-containing lipoplexes. (C-D) At euthanasia, knee (C) and ankle (D) joints were collected and processed for histopathological measurements. (C) Tissue sections were processed for TRAP and hematoxylin staining. Representative sections are shown (20x magnification). The number of TRAP positive osteoclast precursor cells (OCP) and osteoclasts (OC) was counted at the sites of bone erosion. (D) Tissue sections were stained with Safranin O/Fast green for evaluation of bone erosion. Representative sections are shown (20x magnification) and erosion score plotted. (E) MiR-146a^{-/-} (KO) mice were injected i.p. on day 0 and 1 with K/BxN serum to induce arthritis. Mice were injected with miR-146a- or miR-CT-containing lipoplexes at day 4, 7 and 9. Micro-computed tomography analysis was performed for 3-dimensional reconstruction of knee joints and quantification of trabecular micro-architecture of proximal femur bone, including the following parameters: bone specific surface (BS/BV, mm⁻¹) and trabecular thickness (Tb.Th, mm). Data are presented as mean ± SEM of 1-5 technical replicates of 4-5 pooled biological samples (A-B) or of 5-10 individual mice (C-E). Data refer to one representative experiment out of 2. * p<0.05, ** p<0.01, ns: not significant versus controls using Mann-Whitney (A-D), or Kruskal-Wallis (E) tests.

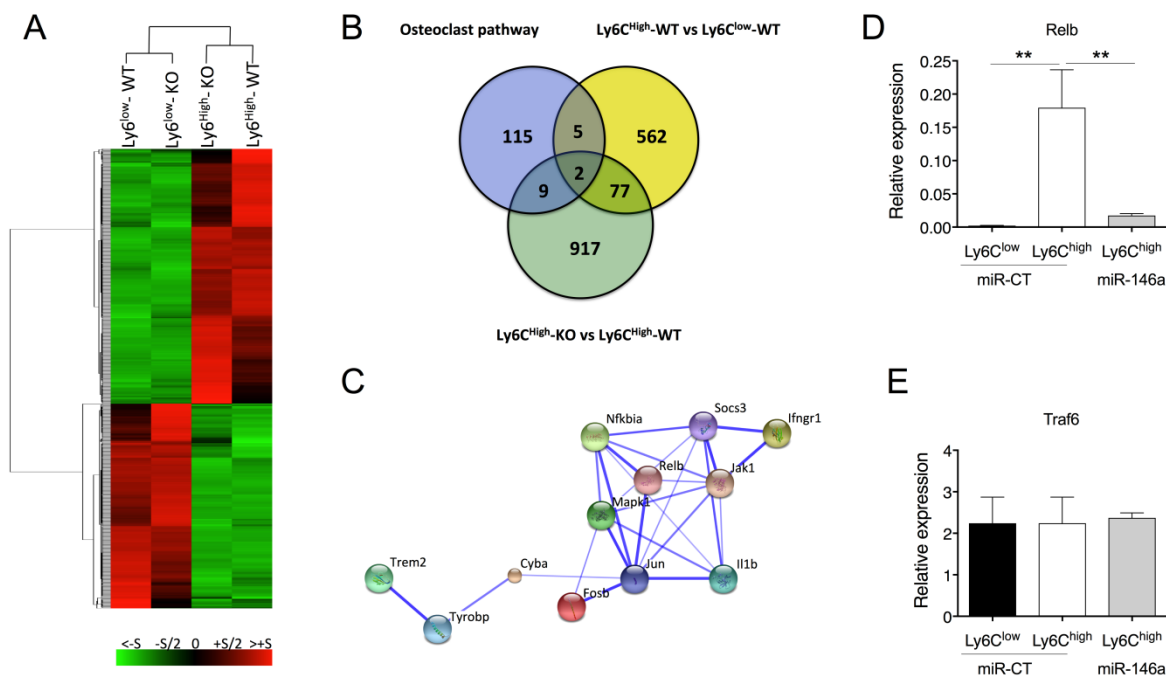


Figure 5. MiR-146a is a regulator of osteoclastogenesis in Ly6C^{high} monocytes. (A) Total RNA was extracted from FACS sorted Ly6C^{high} or Ly6C^{low} blood monocytes isolated from either miR-146a^{-/-} (KO) or wild type (WT) mice (pool of 40 mice/group). After reverse transcription, transcriptomic analysis was performed using mouse GeneChip arrays (Affymetrix). Hierarchical cluster analysis was performed. (B) Venn diagram illustrates the intersection between genes differentially expressed between Ly6C^{high} monocytes of miR-146a^{-/-} (KO) and wild type (WT) mice, genes of the Osteoclast differentiation Pathway SuperPath, and genes differentially expressed between WT Ly6C^{high} and Ly6C^{low} monocytes. (C) STRING analysis generated a confidence view. Thick lines represent strong associations. (D-E) DBA/1 mice were immunized with bovine type II collagen on day 0 and 21, and analyses were performed on day 28. Relative *Relb* (D) and *Traf6* (E) mRNA expression in Ly6C^{high} or Ly6C^{low} splenic monocytes isolated from arthritic mice. The DMAPAP/DOPE cationic liposome was formulated with either miR-146a mimics (0.5mg/kg) (miR-146a, light grey bars) or non-targeting miRNA mimics (miR-CT, black and white bars) and injected twice on day 23 and 27 (pool of 5 mice/group). Mice were sacrificed 24 hours after the last injection and Ly6C^{high} monocytes sorted from pooled spleens (n=2-3 pools of 5 mice/group). Data are presented as mean ± SEM of 3 experimental replicates. ** p<0.01 using Kruskal-Wallis test (D-E).

In vivo, miR-146a targets *RelB* and regulates several osteoclast differentiation components in Ly6C^{high} monocytes

To gain insight into the mechanisms underlying miR-146a-mediated modulation of Ly6C^{high} monocyte function, we compared the expression profiles of Ly6C^{high} and Ly6C^{low} blood monocytes isolated from either miR-146a^{-/-} or WT mice using Affymetrix GeneChip microarrays. Modified HPCDA (High Performance Chip Data Analysis) identified 646 genes significantly differentially expressed between both subsets in wild-type conditions. Surprisingly, 88% of these genes were not affected by miR-146a deficiency, suggesting that miR-146a alone is not sufficient to modify monocyte subset identity (Figure 5A). Focusing on Ly6C^{high} monocytes, we identified 1005 genes differentially regulated according to the miR-146a status. The DAVID functional annotation tool (<http://david.abcc.ncifcrf.gov/>) was then used to identify statistically significant functional associations linking particular gene subsets modulated by miR-146 deficiency in Ly6C^{high} monocytes to specific biological categories (Figure S5). The highest scores included genes related to ribosome, mitochondria, nucleotide process, defense response and RNA processing. None

of these genes were however predicted as direct target of miR-146 when using a high predictive score with at least 3 out of the 4 queried algorithms predicting miRNA target genes (TargetScan, Miranda, RNA22 and miRWalk, data not shown). We then searched for possible relations between these 1005 genes and the 131 genes involved in osteoclast differentiation pathways, as well as with the 646 genes differentially regulated between monocyte subsets. The Venn diagram identified 2 genes at the intersection of the 3 sets (*Mapk1* (alias *Erk*) and *Fosb* (alias AP-1)), as well as 11 genes specific for the OC pathway and affected by miR-146a expression levels in Ly6C^{high} monocytes (Figure 5B). Pathway enrichment analysis was performed with these 11 genes using the web-based bioinformatics application STRING (Search Tool for the Retrieval of Interacting Genes/Proteins). Most of the genes encoded for cytosolic proteins (n=7, p=8.2×10⁻³) and analysis of protein-protein interactions revealed a central role of *Jun* (Figure 5C). Analysis of biological processes showed an involvement of the response to cytokines (n=7, p=1.4 × 10⁻⁵). None of the 11 genes were predicted as direct miR-146a targets, suggesting an indirect miR-146a-mediated regulation.

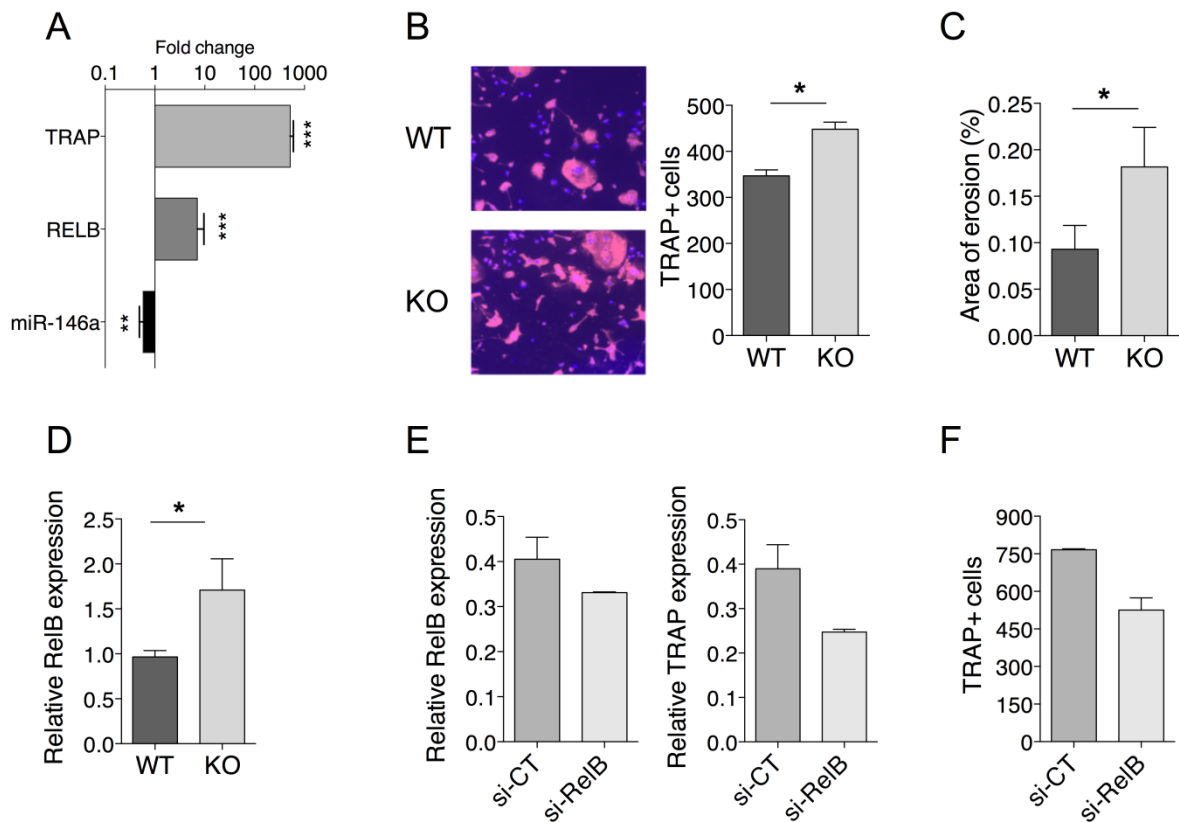


Figure 6. miR-146a controls osteoclast progenitor differentiation through RelB. (A) Primary bone marrow precursors were differentiated by culturing with M-CSF (15 ng/ml) and RANKL (40 ng/ml). Fold change of expression levels of miR-146a, *RelB* and *Trap* gene were quantified during osteoclastogenesis. (B) Osteoclast precursors from miR-146a^{-/-} (KO) mice or wild type littermates (WT) were cultivated in osteoclast differentiation medium for 7 days. Number of TRAP-positive multinucleated osteoclasts was quantified using automated fluorescence imaging (n=20 areas/well, n=4 mice/group). Representative pictures from four independent experiments are shown (10x magnification). (C) Functional assay was performed on an Osteo Assay Surface plate. Relative resorption area was quantified using image J software (n=6 areas/well, two experimental replicates of 4 mice/group pooled). (D) Expression levels of miR-146a were quantified in bone marrow precursors from miR-146a^{-/-} (KO) mice or wild type littermates (WT). (E) miR-146a^{-/-} (KO) mice or wild type (WT) littermates were injected i.p. on day 0 and 1 with K/BxN serum to induce serum-transfer arthritis (STA). The DMAPAP/DOPE cationic liposome was formulated with either CTRL siRNA (si-CT, dark grey bars) or si-RNA targeting *RelB* gene (si-RelB, light grey bars) and injected (0.5mg/kg) twice from day 4 and 7. Mice were sacrificed on day 10. Osteoclast precursors from STA miR-146a^{-/-} (KO) mice injected with siRNA CTRL (si-CT) or siRNA *RelB* (si-RelB) and were cultivated in osteoclast differentiation medium for 7 days. Relative *RelB* and *Trap* mRNA expression was quantified using RTqPCR. (F) Number of TRAP-positive multinucleated osteoclasts was quantified using automated fluorescence imaging (n=20 areas/well, n=4 mice/group). Data are presented as mean \pm SEM, (A) present data from 6 mice/group. Differences between groups were compared using Mann-Whitney test (A, B, C and D). E and F present as mean 2 data from 5 mice/group, no statistical analysis can be carried out. * p<0.05, ** p<0.01, *** p<0.001, ordinary one-way ANOVA t-test.

To mechanistically clarify how miR-146a regulates osteoclast differentiation pathways and contributes to increased OC differentiation of Ly6C^{high} monocyte precursors *in vivo*, we monitored the expression level of two genes that are involved in the canonical and non-canonical OC differentiation pathways and that have been previously validated as miR-146a targets, namely *Relb* and *Traf6* [31, 32]. Consistent with lower levels of miR-146a in Ly6C^{high} than in Ly6C^{low} monocytes, we found higher expression of *Relb* in Ly6C^{high} than in Ly6C^{low} monocytes (Figure 5D). Importantly, we found that miR-146a enforced expression in Ly6C^{high} monocytes in arthritic mice reduced *Relb* transcript levels compared with miR-CT-injected mice. Interestingly, *Traf6* mRNA levels did not vary among conditions (Figure 5E).

miR-146a controls osteoclast progenitor differentiation through *Relb*

To test the hypothesis that reduced miR-146a expression in OCPs promotes OC formation through *Relb*, we first investigated the miR-146a/*Relb* axis during steady state osteoclastogenesis and the effect of miR-146a deficiency in mouse OCPs on OC development. When bone marrow-derived OCPs of miR-146a^{+/+} mice were differentiated into OCs, the expression of miR-146a was down regulated while mRNA levels of the OC marker *Trap* and the *Relb* transcription factor were increased (Figure 6A). Deficiency of miR-146a in OCPs resulted in a significant increase in the number of TRAP positive multinucleated OCs, associated with an increased OC activity, as compared with miR-146a^{+/+} controls (Figure 6B, C). Interestingly, the number of TRAP positive multinucleated OCs obtained from healthy

miR-146a^{-/-} OCPs was comparable to the one obtained from arthritic miR-146a^{+/+} OCPs (Figure 3D). Similar differences were observed with splenic CD11b⁺ OCPs (data not shown). Importantly, the expression level of *Relb* mRNA was significantly increased in OCPs derived from miR-146^{-/-} mice as compared to OCPs from WT mice (Figure 6D). Second, we determined the impact of rescuing miR-146a deficiency in Ly6C^{high} monocytes on OC development and *Relb* expression. When bone marrow (BM) progenitors were collected and cultured under osteoclastogenic conditions, OC differentiation was reduced for miR-146a mimics-treated mice compared with miRNA control-treated mice (Figure S6A). These data were recapitulated *in vitro* when transfecting BM progenitors with miR-146a or miRNA control mimics before inducing osteoclastogenesis (Figure S6B) and reduced osteoclast differentiation was associated with decreased *Relb* mRNA expression (Figure S6C). Finally, we assessed *in vivo* the effect of silencing *Relb* in miR-146a^{-/-} Ly6C^{high} monocytes on osteoclast differentiation. When BM progenitors from siRelB-injected miR-146a^{-/-} arthritic mice were differentiated into OCPs, the expression of *Relb* and *Trap* mRNA were decreased as compared with a siRNA control (Figure 6E), and the number of TRAP positive multinucleated cells reduced as compared with control conditions (Figure 6F). Overall our data suggest that *Relb* silencing in Ly6C^{high} monocytes was able to interfere with increased osteoclastogenesis of miR-146^{-/-} OCPs.

Discussion

Several miRNAs have been reported deregulated in arthritis, being implicated either in inflammation or bone destruction, the two main features of the disease [26]. Among these, miR-146a is described as a negative regulator of both immune responses [46, 47] and osteoclastogenesis [27], thus representing a candidate of choice for therapy in RA [48]. Several groups have described that miR-146a is elevated in unsorted complex tissues, such as blood, synovium or PBMCs, from patients with RA [35, 49, 50]. Paradoxically, significant clinical benefit was obtained on joint pathology using systemic injection of miR-146a in CIA [33]. Here, we specify *in vivo* the cellular context of the beneficial role of miR-146a on bone erosion by demonstrating that enforced expression of miR-146a in Ly6C^{high}, and not in Ly6C^{low}, monocytes efficiently reduced osteoclastogenesis and bone erosion in both STA and CIA arthritis mouse models.

Our data also show that, under arthritic conditions, miR-146a expression in Ly6C^{high} monocytes has no impact on joint inflammation, Ly6C^{high}

frequencies, or cytokine secretion, neither in STA nor in CIA models. This is in line with a previous report showing increased myeloid cell recruitment, joint inflammation and lesions, but no impact on systemic inflammation, in miR-146 KO mice with Lyme-induced arthritis [37]. It is however different from the previous observation that miR-146a negatively regulates Ly6C^{high} monocyte frequency and pro-inflammatory responses [31]. Such discrepancy might be due to the environment and trigger that are different between the study of Etzrodt et al. and ours, i.e. bacterial infection versus arthritis. There are several possible non-exclusive mechanisms that may explain why arthritis severity is increased in full miR-146 KO mice. First, a recent report showed that loss of miR-146a increases the proliferation of synovial fibroblasts (FLS) and the expression of TRAF6 by FLS [38]. Since TRAF6, a known target gene of miR-146, promotes pro-inflammatory cytokine production by FLS isolated from RA patients [51] one can speculate that miR-146 deficiency in FLS may increase local inflammation by removing TRAF6-mediated inhibition on cytokine production and proliferation, two pathogenic features of FLS critically involved in joint inflammation and arthritis severity. Second, mesenchymal stromal cells found in the bone marrow and synovial membrane have the potential to differentiate into a wide range of cell types. They also display immuno-regulatory functions that are lost in presence of TNF and under arthritic conditions [52]. Third, it has been published that Ly6C^{low} monocytes drive joint inflammation [21], constitutively express high levels of miR-146a that cannot be further increased upon LPS challenge, and display higher inflammatory transcriptomic signatures (including components of the NF- κ B signaling cascade) than Ly6C^{high} monocytes when lacking miR-146 [19, 31]. Thus, one can hypothesize that increased arthritis severity observed in miR-146 KO mice might be due to increased inflammatory activation of Ly6C^{low} monocytes. This is sustained by our observation that enforced expression of miR-146a in Ly6C^{high} (but not Ly6C^{low}) monocytes is not effective in reducing arthritis severity and inflammation, neither in CIA nor STA models (Figure S3). Further studies must be conducted to determine the specific role of miR-146 in the Ly6C^{low} monocyte subset.

Our findings suggesting that, in the context of arthritis and miR-146a, Ly6C^{high} monocytes more specifically regulate osteoclastogenesis than inflammation are consistent with previous evidences supporting a role for Ly6C^{high} monocytes in osteoclastogenesis *in vitro* [17, 18] and in bone erosion through bone morphology studies of CCR2^{-/-} mice [53]. Our transcriptomic data reinforce this by showing that,

among genes deregulated in miR-146a^{-/-} Ly6C^{high} monocytes, 11 genes are related to osteoclast differentiation. Interestingly, while the absence of miR-146a in Ly6C^{low} monocytes only affects a hundred genes (data not shown), miR-146a silencing in Ly6C^{high} monocytes modulates the expression of a thousand genes, suggesting that, beyond osteoclastogenesis, miR-146a plays other roles in Ly6C^{high} functions. When performing an enrichment score of the functional annotations to identify predominant biological categories among genes modulated upon miR-146 deficiency, we found totally different gene ontology (GO) processes in both monocyte subsets (Figure S5). Among them, we found GO pathways related to inflammatory response and regulation of cell proliferation in Ly6C^{low} monocytes, and GO pathways related to cellular biosynthetic processes, energy production and mitochondria metabolism in Ly6C^{high} monocytes. Interestingly, the role of mitochondria in osteoclastogenesis has been demonstrated in Relb^{-/-} mice, as well as the critical involvement of the non-canonical Relb signaling cascade for optimal OCs formation [54]. This is in agreement with our results showing that, in Ly6C^{high} monocytes, miR-146a controls *Relb*. In addition, since we also showed that miR-146a does not control *Traf6* in Ly6C^{high} monocytes, it suggests that the negative regulatory role-played by miR-146a in Ly6C^{high} OCP might be through the control of the non-canonical rather than the canonical NK- κ B signalling pathway. Again, these data illustrate the importance of the cellular context when studying miRNA functions, not only the cell identity but also the cellular environment. Our present study illustrates this by showing that the lack of miR-146 in OCP isolated from either arthritic or ovariectomized mice efficiently increases osteoclastogenesis *in vitro*, whereas *in vivo*, increased bone erosion is observed in the context of inflammatory arthritis but not in ovariectomized-induced osteoporosis. These data suggest that the cell-intrinsic effect of miR-146 deficiency in OCP is abolished *in vivo* by environmental factors in ovariectomized-induced osteoporosis and enhanced by inflammatory arthritis condition. This is in line with data from hTNF transgenic arthritic mice transplanted with WT or miR-146^{-/-} bone marrow [38].

Our results suggest a stronger contribution for Ly6C^{high} monocytes than for the Ly6C^{low} subset during CIA development. Using experimental arthritis, we find that Ly6C^{high} monocytes accumulate in the blood and spleen before disease onset, and migrate to the inflamed joints, while the Ly6C^{low} monocyte frequencies remained a minority, and that Ly6C^{high} number in the circulation is associated with increased disease severity. This is in agreement with

previous works depleting Ly6C^{high} monocytes in experimental arthritis with an anti-CCR2 antibody and showing a reduced disease severity, osteoclast formation and bone erosion [55].

In addition, we show that miR-146a is down regulated in Ly6C^{high} monocytes of arthritic mice, as well as in their CD14⁺ human counterparts in RA patients, suggesting that analysis of miR-146a expression levels, specifically in Ly6C^{high} subset, could be used as a bone erosive biomarker in arthritis. Further clinical studies on patients' cohort evaluating correlations between joint MRI and Ly6C^{high}-specific miR-146a expression levels will be required. Using genetic *in vivo* approaches we evidence that the reduced expression level of miR-146a in the Ly6C^{high} subset as compared with the Ly6C^{low} subset is, at least in part, responsible for their more potent osteoclastic potential and increased bone erosion under arthritic conditions. Showing that miR-146a controls Ly6C^{high}-specific dysfunctions in arthritis, our present findings not only provide novel molecular mechanisms that control monocyte subset commitment, but also identify Ly6C^{high} monocytes as a candidate cell target for osteoclast-directed therapy in arthritis. Our data also show that both monocyte subsets display distinct miR-146a expression levels under physiological conditions, which might explain in part their distinct OC differentiation potential.

Conclusions

In conclusion, showing that bone resorption in arthritic joints of miR-146a^{-/-} mice is increased compared to control arthritic miR-146a^{+/+} mice, and that joints of CIA mice are protected from bone erosion when using a Ly6C^{high} subset-specific approach to inhibit osteoclast differentiation of precursors, opens new theranostics perspectives. It also provides a simple way to study at the cellular level how miRNAs are altered during breakdown of tolerance in RA, and to evaluate their therapeutic potential to restore bone homeostasis in arthritis. It underscores the importance of studying the role of other miRNAs in osteoclastogenesis in the context of monocytes' functional heterogeneity. Our work also extends the current knowledge on Ly6C^{high} monocytes, highlighting their predominant role in arthritis as osteoclast precursors responsible for pathological bone resorption, and underscoring the cell-type specific function of miR-146a in osteoclastogenesis *in vivo*. Finally, our data demonstrate the importance of reduced miR-146a expression in the Ly6C^{high} monocyte subset for osteoclast differentiation during inflammatory arthritis and provide evidence that therapeutic delivery of miR-146a mimics to Ly6C^{high}

monocytes represents a possible treatment strategy to interfere with pathogenic bone loss.

Supplementary Material

Supplementary figures.

<http://www.thno.org/v08p5972s1.pdf>

Acknowledgments

We thank Gaelle Cres, Céline Bouclier for technical help on ovariectomy experiments, Rita Vicente and Julie Quentin for technical help during euthanasia, Anne Blangy and Claudine Blin for fruitful discussions on osteoclast biology. Expert technical assistance was provided for histology sections and staining by the Technology facilities of the Biocampus Montpellier (RHEM), for imaging and cell sorting by the Montpellier RIO imaging - IGMM - Cytometry plateforme (MRI), for animal husbandry and functional investigations by Montpellier animal facility network (RAM), as well as for microCT scanner by the National plateforme eCellFrance. Affymetrix microarrays were processed in the Microarray Core Facility of the Institute in Regenerative Medicine and Biotherapy, CHU-INSERM-University of Montpellier (<http://www.chu-montpellier.fr/fr/irmb/>).

Fundings

This work was supported by INSERM (Institut National de la Santé et Recherche Médicale), the University of Montpellier, the Arthritis Fondation Courtin, the European union (grant number 115142), the E-Rare-3 Joint Transnational Research Project on Rare Diseases INSAID that is a merged initiative between EC and ANR (ANR-15-RAR3-0013-05) and the Fondation pour la Recherche Médicale.

Authors' contributions

MA designed and performed the experiments, analyzed data, and contributed to the writing. JP performed kinetic studies of the monocyte subsets in the CIA mouse model, cell sorting and cytometric analysis of mouse samples, analyzed and interpreted data, and contributed in building the figures. CP performed RT-qPCR quantifications and analysis. GR and CR performed the quantification of TRAP+ osteoclasts *in vitro* and *in vivo*, and analyzed the data. VE developed the miR mimics delivery system. KT performed *in vivo* bone histomorphometric experiments and analysis. ALB performed CIA experiments and *in vivo* bone histomorphometric measurements, and provided her expertise for statistical analyses of the data presented. MC and MR performed ELISA experiments and analysis. PG and RN provided samples for mouse STA experiments. LT provided samples for human data sets. JRG, TH, and AG

performed the microarray data analyses. YMP and CJ provided human samples. IDR contributed to data acquisition, analysis, and interpretation, and assembled the figures. FA and GC supervised the work, designed the study, analyzed and interpreted the data, and drafted the manuscript. All authors have been involved in reading and editing the manuscript, and approved the final version.

Competing Interests

The authors have declared that no competing interest exists.

References

- [1] Boissier M-C, Semerano L, Challal S, et al. Rheumatoid arthritis: from autoimmunity to synovitis and joint destruction. *J Autoimmun.* 2012; 39: 222-8.
- [2] Kourilovitch M, Galarza-Maldonado C, Ortiz-Prado E. Diagnosis and classification of rheumatoid arthritis. *J Autoimmun.* 2014; 48-49: 26-30.
- [3] Kinne RW, Stuhlmüller B, Burmester GR. Cells of the synovium in rheumatoid arthritis. *Macrophages. Arthritis Res Ther.* 2007; 9: 224.
- [4] Herenius MM, Thurlings RM, Wijbrandts CA, et al. Monocyte migration to the synovium in rheumatoid arthritis patients treated with adalimumab. *Ann Rheum Dis.* 2011; 70: 1160-2.
- [5] Evans HG, Gullick NJ, Kelly S, et al. In vivo activated monocytes from the site of inflammation in humans specifically promote Th17 responses. *Proc Natl Acad Sci U S A.* 2009; 106: 6232-7.
- [6] Egan PJ, van Nieuwenhuijze A, Campbell IJ, et al. Promotion of the local differentiation of murine Th17 cells by synovial macrophages during acute inflammatory arthritis. *Arthritis Rheumatol.* 2008; 58: 3720-9.
- [7] Schett G, Gravalles E. Bone erosion in rheumatoid arthritis: mechanisms, diagnosis and treatment. *Nat Rev Rheumatol.* 2012; 8: 656-64.
- [8] Zhu B, Bando Y, Xiao S, et al. CD11b+Ly-6C(hi) suppressive monocytes in experimental autoimmune encephalomyelitis. *J Immunol.* 2007; 179: 5228-37.
- [9] Shi C, Pamer EG. Monocyte recruitment during infection and inflammation. *Nat Rev Immunol.* 2011; 11: 762-74.
- [10] Tak PP, Kalden JR. Advances in rheumatology: new targeted therapeutics. *Arthritis Res Ther.* 2011; 13 (Suppl 1):S5.
- [11] Hamilton JA, Tak PP. The dynamics of macrophage lineage populations in inflammatory and autoimmune diseases. *Arthritis Rheumatol.* 2009; 60: 1210-21.
- [12] Haringman JJ, Gerlag DM, Zwiderman AH, et al. Synovial tissue macrophages: a sensitive biomarker for response to treatment in patients with rheumatoid arthritis. *Ann Rheum Dis.* 2005; 64: 834-8.
- [13] Auffray C, Sieweke MH, Geissmann F. Blood monocytes: development, heterogeneity, and relationship with dendritic cells. *Annu Rev Immunol.* 2009; 27: 669-92.
- [14] Ingersoll MA, Platt AM, Potteaux S, et al. Monocyte trafficking in acute and chronic inflammation. *Trends Immunol.* 2011; 32: 470-7.
- [15] Gordon S, Taylor PR. Monocyte and macrophage heterogeneity. *Nat Rev Immunol.* 2005; 5: 953-64.
- [16] Cros J, Cagnard N, Woollard K, et al. Human CD14dim monocytes patrol and sense nucleic acids and viruses via TLR7 and TLR8 receptors. *Immunity.* 2010; 33: 375-86.
- [17] Seeling M, Hillenhoff U, David JP, et al. Inflammatory monocytes and Fcγ receptor IV on osteoclasts are critical for bone destruction during inflammatory arthritis in mice. *Proc Natl Acad Sci U S A.* 2013; 110: 10729-34.
- [18] Jacome-Galarza CE, Lee SK, Lorenzo JA, et al. Identification, characterization, and isolation of a common progenitor for osteoclasts, macrophages, and dendritic cells from murine bone marrow and periphery. *J Bone Miner Res.* 2013; 8: 1203-13.
- [19] Swirski FK, Nahrendorf M, Etzrodt M, et al. Identification of splenic reservoir monocytes and their deployment to inflammatory sites. *Science.* 2009; 325: 612-6.
- [20] Cook AD, Turner AL, Braine EL, et al. Regulation of systemic and local myeloid cell subpopulations by bone marrow cell-derived granulocyte-macrophage colony-stimulating factor in experimental inflammatory arthritis. *Arthritis Rheumatol.* 2011; 63: 2340-51.
- [21] Misharin AV, Cuda CM, Saber R, et al. Nonclassical Ly6C(-) Monocytes Drive the Development of Inflammatory Arthritis in Mice. *Cell Rep.* 2014; 9: 591-604.
- [22] Puchner A, Saferding V, Bonelli M, et al. Non-classical monocytes as mediators of tissue destruction in arthritis. *Ann Rheum Dis.* 2018; 77: 1490-7.
- [23] Patel SK, Janjic JM. Macrophage targeted therapeutics as personalized nanomedicine strategies for inflammatory diseases. *Theranostics.* 2015; 5: 150-72.
- [24] Lagos-Quintana M, Rauhut R, Lendeckel W, et al. Identification of novel genes coding for small expressed RNAs. *Science.* 2001; 294: 853-8.

- [25] Filipowicz W, Bhattacharyya SN, Sonenberg N. Mechanisms of post-transcriptional regulation by microRNAs: are the answers in sight? *Nat Rev Genet.* 2008; 9: 102-14.
- [26] Duroux-Richard I, Jorgensen C, Apparailly F. What do microRNAs mean for rheumatoid arthritis? *Arthritis Rheumatol.* 2012; 64: 11-20.
- [27] Kagiya T, Nakamura S. Expression profiling of microRNAs in RAW264.7 cells treated with a combination of tumor necrosis factor alpha and RANKL during osteoclast differentiation. *J Periodontol Res.* 2013; 48: 373-85.
- [28] Franceschetti T, Kessler CB, Lee SK, et al. miR-29 promotes murine osteoclastogenesis by regulating osteoclast commitment and migration. *J Biol Chem.* 2013; 88: 33347-60.
- [29] Krzeszinski JY, Wei W, Huynh H, et al. miR-34a blocks osteoporosis and bone metastasis by inhibiting osteoclastogenesis and Tgif2. *Nature.* 2014; 512: 431-5.
- [30] de la Rica L, García-Gómez A, Comet NR, et al. NF- κ B-direct activation of microRNAs with repressive effects on monocyte-specific genes is critical for osteoclast differentiation. *Genome Biol.* 2015; 16: 2.
- [31] Etzrodt M, Cortez-Retamozo V, Newton A, et al. Regulation of monocyte functional heterogeneity by miR-146a and Relb. *Cell Rep.* 2012; 1: 317-24.
- [32] Taganov KD, Boldin MP, Chang KJ, et al. NF- κ B-dependent induction of microRNA miR-146, an inhibitor targeted to signaling proteins of innate immune responses. *Proc Natl Acad Sci U S A.* 2006; 103: 12481-6.
- [33] Nakasa T, Shibuya H, Nagata Y, et al. The inhibitory effect of microRNA-146a expression on bone destruction in collagen-induced arthritis. *Arthritis Rheumatol.* 2011; 63: 1582-90.
- [34] Nakasa T, Miyaki S, Okubo A, et al. Expression of microRNA-146 in rheumatoid arthritis synovial tissue. *Arthritis Rheumatol.* 2008; 58: 1284-92.
- [35] Murata K, Yoshitomi H, Tanida S, et al. Plasma and synovial fluid microRNAs as potential biomarkers of rheumatoid arthritis and osteoarthritis. *Arthritis Res Ther.* 2010; 12: R86.
- [36] Stanczyk J, Pedrioli DM, Brentano F, et al. Altered expression of MicroRNA in synovial fibroblasts and synovial tissue in rheumatoid arthritis. *Arthritis Rheumatol.* 2008; 58: 1001-9.
- [37] Lochhead RB, Ma Y, Zachary JF, et al. MicroRNA-146a provides feedback regulation of lyme arthritis but not carditis during infection with *Borrelia burgdorferi*. *PLoS Pathog.* 2014; 10: e1004212.
- [38] Saferding V, Puchner A, Goncalves-Alves E, et al. MicroRNA-146a governs fibroblast activation and joint pathology in arthritis. *J Autoimmun.* 2017; 82: 74-84.
- [39] Presumey J, Courties G, Louis-Plence P, et al. Nicotinamide phosphoribosyltransferase/visfatin expression by inflammatory monocytes mediates arthritis pathogenesis. *Ann Rheum Dis.* 2013; 72: 1717-24.
- [40] Charbonnier LM, Han WG, Quentin J, et al. Adoptive transfer of IL-10-secreting CD4⁺CD49b⁺ regulatory T cells suppresses ongoing arthritis. *J Autoimmun.* 2010; 34: 390-9.
- [41] Brazier H, Stephens S, Ory S, et al. Expression profile of RhoGTPases and RhoGEFs during RANKL-stimulated osteoclastogenesis: identification of essential genes in osteoclasts. *J Bone Miner Res.* 2006; 21: 1387-98.
- [42] Biesen R, Demir C, Barkhudarova F, et al. Sialic acid-binding Ig-like lectin 1 expression in inflammatory and resident monocytes is a potential biomarker for monitoring disease activity and success of therapy in systemic lupus erythematosus. *Arthritis Rheumatol.* 2008; 58: 1136-45.
- [43] Belinky F, Nativ N, Stelzer G, et al. PathCards: multi-source consolidation of human biological pathways. *Database (Oxford);* 2015:2015.
- [44] Jakubzick C, Gautier EL, Gibbings SL, et al. Minimal differentiation of classical monocytes as they survey steady-state tissues and transport antigen to lymph nodes. *Immunity.* 2013; 39: 599-610.
- [45] Monach P, Hattori K, Huang H, et al. The K/BxN mouse model of inflammatory arthritis: theory and practice. *Methods Mol Med.* 2007; 136: 269-82.
- [46] Boldin MP, Taganov KD, Rao DS, et al. miR-146a is a significant brake on autoimmunity, myeloproliferation, and cancer in mice. *J Exp Med.* 2011; 208: 1189-201.
- [47] Zhao JL, Rao DS, O'Connell RM, et al. MicroRNA-146a acts as a guardian of the quality and longevity of hematopoietic stem cells in mice. *Elife.* 2013; 2: e00537.
- [48] Ammari M, Jorgensen C, Apparailly F. Impact of microRNAs on the understanding and treatment of rheumatoid arthritis. *Curr Opin Rheumatol.* 2013; 25: 225-33.
- [49] Pauley KM, Satoh M, et al. Upregulated miR-146a expression in peripheral blood mononuclear cells from rheumatoid arthritis patients. *Arthritis Res Ther.* 2008; 10: R101.
- [50] Li J, Wan Y, Guo Q, et al. Altered microRNA expression profile with miR-146a upregulation in CD4⁺ T cells from patients with rheumatoid arthritis. *Arthritis Res Ther.* 2010; 12: R81.
- [51] Zhu LJ, Yang TC, Wu Q, et al. Tumor necrosis factor receptor-associated factor (TRAF) 6 inhibition mitigates the pro-inflammatory roles and proliferation of rheumatoid arthritis fibroblast-like synoviocytes. *Cytokine.* 2017; 93: 26-33.
- [52] Djouad F, Fritz V, Apparailly F, et al. Reversal of the immunosuppressive properties of mesenchymal stem cells by tumor necrosis factor alpha in collagen-induced arthritis. *Arthritis Rheumatol.* 2005; 2: 1595-603.
- [53] Binder NB, Niederreiter B, Hoffmann O, et al. Estrogen-dependent and C-C chemokine receptor-2-dependent pathways determine osteoclast behavior in osteoporosis. *Nat Med.* 2009; 15: 417-24.
- [54] Zeng R, Faccio R, Novack DV. Alternative NF- κ B Regulates RANKL-Induced Osteoclast Differentiation and Mitochondrial Biogenesis via Independent Mechanisms. *J Bone Miner Res.* 2015; 30: 2287-99.
- [55] Brühl H, Cihak J, Plachý J, et al. Targeting of Gr-1⁺,CCR2⁺ monocytes in collagen-induced arthritis. *Arthritis Rheumatol.* 2007; 56: 2975-85.